1 Characterizing the automatic radon flux Transfer Standard
2 system *Autoflux*: laboratory calibration and field experiments

3 Claudia Grossi[1,2], Daniel Rabago[3], Scott Chambers[4], Carlos Sáinz[3], Roger Curcoll[1], Peter PS.
4 Otáhal[5], Eliška Fialová[5,6], Luis Quindos[3], Arturo Vargas[1]

6 [1] Institut de Tècniques Energètiques, Universitat Politècnica de Catalunya, 08028 Barcelona, Spain
7 [2] Physics Department, Universitat Politècnica de Catalunya,08028 Barcelona, Spain
8 [3] Universidad de Cantabria, 39011 Santander, Spain
9 [4] ANSTO, Environmental Research, Lucas Heights, NSW 2234, Australia
10 [5] Nuclear Protection Department, National Institute for Nuclear, Chemical & Biological Protection, Milin 26231,
11 Czech Republic
12 [6] Department of Geological Sciences, Faculty of Science, Masaryk University, 60200 Brno, Czech Republic

13 *Correspondence to*: Claudia Grossi (claudia.grossi@upc.edu)

15 **Abstract**

17 High-quality, long-term measurements of terrestrial trace gas emissions are important for investigations of
18 atmospheric, geophysical and biological processes to help mitigate climate change, protect the environment, and
19 the health of citizens. High-frequency terrestrial fluxes of the radioactive noble gas ^{222}Rn, in particular, are useful
20 for validating radon flux maps, used to evaluate the performance of regional atmospheric models, to improve
21 greenhouse gas emission inventories (by the Radon Tracer Method) and to determine Radon Priority Areas for
22 radiation protection goals.

24 A new automatic radon flux system (the *Autoflux*) was developed as a Transfer Standard (TS) to assist with
25 establishing a traceability chain for field-based radon flux measurements. The operational characteristics and
26 features of the system were optimized based on a literature review of existing flux measurement systems. To
27 characterize and calibrate the *Autoflux* a bespoke radon Exhalation Bed (EB) facility was also constructed with the
28 intended purpose of providing a constant radon emanation under a specific set of controlled laboratory conditions.
29 The calibrated *Autoflux* was then used to transfer the derived calibration to a second continuous radon flux system
30 under laboratory conditions, both instruments were then tested in the field and compared with modeled fluxes.

32 This paper presents: i) a literature review of state-of-the-art radon flux systems and EB facilities; ii) the design,
33 characterization and calibration of a reference radon EB facility; iii) the design, characterization and calibration of
34 the *Autoflux* system; iv) the calibration of a second radon flux system (*INTE_Flux*) using the EB and *Autoflux*,
35 with a total uncertainty of 9% (k=1) for an average radon flux of ~1800 mBq m^{-2} s^{-1} under controlled laboratory
36 conditions; and iv) an example application of the calibrated TS and *INTE_Flux* systems for in situ radon flux
37 measurements which are then compared with simulated radon fluxes. Calibration of the TS under different
38 environmental conditions and at lower reference fluxes will be the subject of a separate future investigation.

40 1 Introduction

42 The noble, radioactive gas radon (^{222}Rn) contributes over half of the total public radiation dose from natural sources
43 (WHO, 2009). However, due to its short half-life (3.8 days) and chemical inertness, radon is also widely used as
44 an environmental tracer for atmospheric and geophysical processes (Grossi et al., 2012; Vargas et al., 2015,
45 Chambers et al., 2016; Chambers et al., 2018; Zhang et al., 2021). In particular, climate scientists are using co-
46 located measurements of atmospheric radon and greenhouse gas (GHG) concentrations to apply the so-called
47 Radon Tracer Method (RTM) for estimating local- to regional-scale GHG emissions (Grossi et al., 2018; Levin et
48 al., 2021).

49 These applications require information, at high temporal resolution and low uncertainty, about: i) the quantity of
50 radon emitted per unit area and time from a surface of interest (the radon flux, *F*, or exhalation rate; usually
51 expressed in mBq m^{-2} s^{-1}); and ii) the atmospheric radon activity concentration (SI units Bq m^{-3}).

52 Terrestrial radon exhalation is the result of ^{222}Rn escape from soil pore spaces to the atmosphere after its formation
53 by ^{226}Ra decay (Nazaroff, 1992). ^{222}Rn exhalation rates are primarily driven by diffusion processes and depend
54 strongly on the soil ^{226}Ra content and soil properties (porosity, tortuosity, soil humidity, etc.). Consequently, the
55 ^{238}U content and parameters influencing diffusive transport in the soil need to be known to properly estimate the

56 spatial and temporal variability of ^{222}Rn exhalation rates (Schüßler, 1996; Lopez-Coto et al., 2013; Karstens et al.,
57 2015). Furthermore, the emanation factor of radon from the soil grains to the pore spaces is influenced by soil
58 humidity (Nazaroff, 1992; Zhuo et al., 2006; Zhuo et al., 2008).

59 Although diffusion is the primary transport mechanism of radon in soils, driven by the strong vertical concentration
60 gradient (Karstens et al., 2015), advective transport can also occur, but this has not been thoroughly investigated
61 and is likely to be highly site specific. Advective transport typically results from local pressure gradients, changing
62 wind speed and direction, etc. Consequently, advective processes could influence radon flux measurements
63 (Gutiérrez-Álvarez et al. 2020a). Other factors including soil type, atmospheric pressure, rainfall (related to soil
64 moisture), and soil temperature can affect the radon flux. However, complex dependencies between these factors
65 makes it difficult to quantify changes in radon flux due to any one of these factors in isolation (e.g., a precipitation
66 event is often also associated with a drop in pressure and temperature).

67 To date, most radon flux studies have been based on random sampling and short temporal measurement data, due
68 to the lack of robust continuous radon flux systems. Unfortunately, these kinds of datasets are not sufficient to
69 clarify relationships between radon flux and environmental factors. This is also a contributing factor to why some
70 studies reach contradictory conclusions about the influence of individual parameters on the radon flux.

71 Long-term, reliable radon flux measurements are needed in conjunction with corresponding environmental
72 observations in the soil and lower atmosphere (McLaughlin, 2011; Yang et al., 2017). To ensure reliable
73 measurements it is important to characterize and calibrate the operational radon flux systems, which requires: i) a
74 ^{222}Rn Exhalation Bed (EB) facility, to provide reference radon fluxes under controlled laboratory conditions; ii) a
75 Transfer Standard (TS) instrument to be calibrated using the EB and used as a reference monitor for calibrating
76 other new or existing monitors, or to be used directly for in situ measurement campaigns; and iii) planned field-
77 based inter-comparison campaigns of different radon flux systems under in situ environmental conditions.

78 One of the main aims of the EMPIR 19ENV01 project (henceforth traceRadon), which started in June 2020, was
79 to provide the necessary measurement infrastructure and transfer standards to enable traceable radon flux and
80 atmospheric radon activity concentration measurements. These goals are being achieved in collaboration with,
81 among other research groups, the Integrated Carbon Observation System (ICOS, www.icos-cp.eu) network, whose
82 researchers are interested in introducing treaceable radon flux and atmospheric radon concentration measurements
83 to sites within this network for RTM applications.

84 The specific contributions of this study to the overall traceRadon objectives are to offer a calibrated and
85 characterized continuous TS system, provided with soil and atmosphere sensors, that can be used to carry out
86 radon flux campaigns at different sites to help improve and evaluate the performance of contemporary radon flux
87 maps and models (Szegvary et al., 2009; Karstens et al., 2015), as well as be used to calibrate other radon flux
88 systems under laboratory or field conditions.

89 The remainder of this manuscript is arranged in the following way: first, a review is made of state-of-the-art EB
90 facilities, including a description of the one newly designed, built and characterized by Cantabria University for
91 the traceRadon project; next, a review is presented of contemporary, available state-of-the-art radon flux systems,
92 including a description of the new automated system (*AutoFlux*) designed, characterized and calibrated by the
93 Australian Nuclear Science and Technology Organization (ANSTO) and the Universitat Politècnica de Catalanuya
94 (UPC); next, the protocol applied to calibrate another automatic radon flux system (*INTE_Flux*), designed by the
95 Institute of Energy Technologies of the UPC, using the *AutoFlux* and the UC EB facility is described. Finally, both
96 radon flux systems are tested during a field-based intercomparison campaign and the results compared with
97 previous tests of these systems and with radon flux model outputs available at the ICOS Carbon Portal (www.icos-
98 cp.eu/).

99

2 Materials and Methods

2.1. Overview of theoretical radon flux estimation

104 A review of relevant literature found that radon flux studies have historically been carried out using a theoretical
105 value as a reference. IAEA (1992) suggested that radon flux systems should be calibrated using a thin layer model,

106 under the assumption of 'pure' diffusion and a soil with well characterized ^{226}Ra activity concentration, depth
107 (thickness), porosity, and radon emanation characteristics (UNSCEAR, 1988; Rogers & Nielson, 1991; Nazaroff,
108 1992; Porstendörfer, 1994). In contrast, most contemporary radon flux studies have been based on the experimental
109 accumulation chamber method (Hassan et al., 2009), resulting in a standard method reflected in the ISO 11665-
110 7:2012: *Accumulation method for estimating surface exhalation rate*. In these cases, the reference value used for
111 calibration of the radon flux system, and method of flux measurement, is based on the results of an exponential fit
112 of the increasing radon activity concentration inside a chamber of known volume, or in a STAR (System for Test
113 Atmospheres with Radon) (ISO, 2009), during several days.

114 The theoretical approach enables calculation of the radon flux (F) by the diffusion equation (Porstendörfer, 1994):

$$F = \varepsilon \cdot C_{\mathrm{Ra}} \cdot \rho \cdot L \cdot \lambda \cdot \tanh\left(\frac{z}{L}\right) \qquad (1)$$

115 where ε is the radon emanation factor, C_{Ra} is the ^{226}Ra activity of the soil (Bq kg^{-1}), ρ the dry bulk density (kg m^{-3})
116 of the soil, L the radon diffusion length in the soil (m), z is the soil thickness (m) and λ is the radon decay
117 constant ($2.0993 \cdot 10^{-6}$ s^{-1}).

118 Within Eq. 1, the emanation factor is defined to be the fraction of radon atoms produced by radium disintegration
119 that escape into the soil pore space. Its value varies between 0, when radon does not escape the ^{226}Ra-containing
120 soil grain, and 1, when all radon escapes. This factor depends on many things, including: grain size and shape,
121 moisture content, porosity, permeability, and the distribution of ^{226}Ra atoms in the mineral grains (Baskaran, 2016).

122 Considering a soil sample of a determinate mass, the emanation factor ε can be defined as:

$$\varepsilon = \frac{A_{\mathrm{Rn}}}{A_{\mathrm{Ra}}} \qquad (2)$$

123 where A_{Ra} is the total radium activity of the sample, and A_{Rn}, the radon activity that escapes from the sample. The
124 radium activity is usually measured by gamma spectrometric analysis of the soil sample (i.e., Quindos et al., 1994).
125 To determine the radon activity that escapes from the sample, an airtight stainless-steel container of known volume
126 is commonly used, and the rate of escape is determined by the increase in radon concentration inside (i.e., Stoulos
127 et al., 2004). The sample has to be sufficiently well distributed to ensure that all radon atoms successfully entering
128 the pore spaces of the sample will eventually escape to the air volume and be measured.

129 The bulk density, ρ, can be calculated from the sample weight and volume of the dry soil (Hosoda, 2007). When
130 the soil thickness is much smaller than the radon diffusion length (i.e., $z \ll L$), as is the case for the Exhalation
131 Bed used in this study, the approximation $\tanh(z/L) \approx z/L$ can be used. Thus, the final equation will be (Lopez-
132 Coto et al., 2009):

$$F = \varepsilon \cdot C_{\mathrm{Ra}} \cdot \rho \cdot \lambda \cdot z \qquad (3)$$

133 In order to prove the applicability of Eq. 3, the diffusion length L has to be evaluated and compared with z. L can
134 be estimated as:

$$L = \sqrt{D/\lambda} \qquad (4)$$

135 where D is the effective diffusion coefficient of the trace gas in the soil air (hereafter also named effective
136 diffusivity). D is assumed to be constant with depth (Karstens et al., 2015), and can be estimated from water
137 saturation w_s and porosity p using the following expression (Rogers and Nielson, 1991; Prasad et al., 2012):

$$D = D_{air} \cdot p \cdot \exp(-6 w_s p - 6 w_s{}^{14p}) \qquad (5)$$

138 where D_{air} is the radon diffusion coefficient in air ($1.1 \cdot 10^{-5}$ m^{2}s^{-1}).

139 Karstens et al., (2015) made reference to Jin and Jury (1996) and Millington and Quirk (1960) who proposed, and
140 verified, another experimental estimation of the effective diffusivity:

$$D = D_{air} \cdot \frac{(p - w_V)^2}{p^{2/3}} \qquad (5a)$$

142 where w_V (m^3/m^3) is the Volume Water Content (VWC) of the soil. Equations 5 and 5a were both derived
143 empirically and are quite consistent with each other, mainly for dry soils, as will be shown in the following sections.

144 The porosity and water saturation w_s (m³/m³) (Idoria et al., 2020; IAEA, 2013) are given by:

$$p = 1 - \frac{\rho}{\rho_g} \tag{6}$$

145 where ρ_g is the grain density, and:

$$w_s = \frac{\rho \cdot w_c}{p \cdot \rho_w} \tag{7}$$

146

147 where w_c (kg/kg) is the mass water content of the soil sample and ρ_w is the water density (1000 kg/m³). Karstens
148 et al., (2015) reported that the temperature dependence of ²²²Rn diffusivity could also be estimated according to
149 Schery and Wasiolek (1998):

$$D(T) = D_0 \left(\frac{T}{T_0}\right)^{3/2} \tag{8}$$

150

151 where T is the mean soil temperature in Kelvin and D_0 the effective diffusivity at the reference temperature $T_0=$
152 273 K.

153 The experimental approach allows the flux of a given soil surface to be calculated from the increase in radon
154 activity concentration $C_{\text{Rn}}(t)$ within a chamber of known volume during a time t, as described by Eq. 9:

$$C_{\text{Rn}}(t) = C_0 e^{-\lambda_{eff} t} + \frac{F \cdot A}{V_{eff} \cdot \lambda} \left(1 - e^{-\lambda_{eff} t}\right) \tag{9}$$

155

156 where the effective decay constant, λ_{eff}, is the sum of the radon decay constant (λ), possible radon lost due to system
157 leakages (λ_l), and radon concentration reabsorbed by the ground (λ_r), as described by Grossi et al., (2011). C_0 is
158 the initial radon activity concentration within the volume, V_{eff} is the effective volume where the radon is free to
159 accumulate, and A is the area of the exhaling surface.

160

2.2. State of the art Exhalation Bed facilities
162

163 Table S1 in the supplementary material presents a summary of EB facilities found in the literature. The Canadian
164 Mining Institute (CANMET) built a national reference standard flux bed for calibrating flux monitoring
165 instrumentation. This 5 m diameter bed consisted of a 5.5 cm thick layer of uranium bearing material from uranium
166 tailings and provided a radon flux of 285 ± 41 mBq m⁻² s⁻¹ (Stieff et al., 1996). In the University of South China
167 Radon Laboratory a standard facility simulating radon exhalation from soil was built in 2001 (Tan & Xiao, 2011).
168 It consisted of a radon source located at the bottom of a conical volume. The middle cylindrical part was made of
169 a plaster and spumy board that simulates the soil or sand porosity. Finally, in the upper part, there is powdery
170 calcium carbonate to maintain the radon concentration in the conical volume. The reference flux for this system is
171 1482 ± 50 mBq m⁻² s⁻¹, which was measured using an activated charcoal box and Lucas cells. It is still operating,
172 and some studies continue to use it (Tan & Xiao, 2013; Tan et al., 2020). Oak Ridge Associated Universities
173 (Tennessee, USA) constructed a multilayer exhalation bed. It consists of a base layer of uranium ore spread over
174 the bottom of a rectangular Hardigg polyethylene case of dimensions 84 cm × 53 cm. The base has a 10 cm
175 covering layer of dirt to create a uniform flux at the top surface. The reference exhalation rate of this system was
176 determined by the accumulation method, using a continuous radon monitor, and by using activated charcoal
177 canisters and electrets. The range of values obtained varied from approximately 80 mBq m⁻² s⁻¹ to 430 mBq m⁻² s⁻¹
178 ¹ (Altic, 2014). Onishchenko et al. (2015), from the Institute of Industrial Ecology UB RAS (Ekaterinburg, Russia),
179 designed a calibration system to test radon flux measurement devices. It was constructed from a 200 L metal drum
180 filled with quartz sand (radium concentration less than 2.5 Bq/kg) with a calibrated ²²⁶Ra source in the bottom
181 space of the system. The reference exhalation rate obtained by the accumulation method and charcoal canisters
182 was 700 ± 80 mBq m⁻² s⁻¹.

183 Gutiérrez-Álvarez et al. (2020a; 2020b) performed an experimental characterization of a soil exhalation rate using
184 the accumulation method (Eq. 9). Two reference exhalation soils were prepared using phosphogypsum in
185 rectangular polypropylene boxes with 6.0 cm and 13.0 cm soil thicknesses, respectively. Experimental estimates

186 of the exhalation rate of 13.3 ± 0.2 mBq m⁻² s⁻¹ and 23.4 ± 0.3 mBq m⁻² s⁻¹ were determined. These results were
187 compared to exhalation rates determined by applying the theoretical approach and no statistical difference was
188 noted between the two methodologies used.

2.3. Design of a Reference Radon Exhalation Bed

192 In the framework of traceRadon, and using information from the previous section, a radon EB was designed and
193 built at the University of Cantabria (UC) following Gutiérrez-Álvarez et al. (2020a; 2020b). The EB structure
194 consisted of five stainless steel plates, welded in the shape of a box, open at the top. In this configuration it is
195 important to minimize air leakages through the plates that may lead to the loss of radon activity. The intended
196 purpose of this EB was to provide a constant, well characterized, radon emanation rate under a specific set of
197 controlled laboratory conditions. Since soil moisture influences on the radon emanation were not of specific
198 interest in this case, a relatively shallow soil matrix was sufficient for the EB aims.

199 The EB structure was filled with a high ^{226}Ra content soil, extracted from a former Spanish uranium mine in
200 Saelices el Chico (Spain), managed by the Spanish National Uranium Company ENUSA. A total soil mass of
201 around 400 kg was collected. The material was then transported to UC laboratory and distributed over a 30 m²
202 plastic surface in a layer of thickness of approximately 1 cm to be dried and homogenized. Soil homogenization
203 was performed according to technical document 1415 (IAEA, 2004) following these steps: i) the material was
204 manually homogenized using a stainless-steel rake; and ii) it was sieved with a 2 mm aperture sieve (the device
205 has a woven wire mesh in accordance with DIN ISO 3310-1). For the sieving process, soil was taken randomly in
206 5 kg amounts. Finally, the homogenized soil was placed into the EB container.

207 The EB facility was installed in the basement of the UC Faculty of Medicine, in the Laboratory of Environmental
208 Radioactivity (LaRUC). Sensors were installed to continuously monitor temperature, pressure and soil moisture.
209 Two thermometers (Testo, Model 175T2) measured the soil temperature and air temperature inside the
210 accumulation chambers. Soil moisture was measured with an ODYSSEY (Xtreem) probe, and all environmental
211 parameters were recorded by a data logger every minute. Table S2 of the supplementary material summarizes the
212 main characteristics of the selected sensors.

213 The EB radon flux was estimated theoretically and experimentally using the approaches presented in Section 2.1.
214 To apply Eq. 3, the various soil parameters were measured and/or calculated as explained in Section 3. The
215 experimental derivation of the EB's radon flux was performed using Eq. 9 as by Gutiérrez-Álvarez et al. (2020a).
216 For this, the whole surface of the EB was covered with a stainless-steel container of known volume (Figure S1 of
217 the supplementary material). Three radon monitors, an RTM 2200 (Sarad GmbH), a Radon Scout (Sarad GmbH)
218 and an AlphaE (Bertin Instruments), were used simultaneously to measure the increase of radon concentration
219 within the effective accumulation volume. Please note that the sum of the volumes occupied by the solid
220 components of the three monitors were lower than 1% of the total available volume of the used accumulation
221 chamber. In addition, several small air samples were also taken using the grab sampling technique and analysed
222 with the ionization chamber IK-250 (RADON v.o.s.).

2.4. State of the art in Radon Flux Systems

226 A literature review carried out in the framework of traceRadon found that radon monitors employed in flux
227 measurement systems mainly fall into two categories: active or passive. Active monitors analyze the air in real
228 time, whereas passive monitors (i.e., charcoal canisters) rely on the progressive accumulation of radon by
229 diffusion. The accumulated radon is then measured using a separate system (e.g., by gamma spectroscopy or ion
230 chamber) (McLaughlin, 2011). Due to the need of radon flux systems capable of high-frequency measurements
231 (capable of resolving diurnal variability), only active systems will be presented and discussed here.

232 Generally, radon flux systems are comprised of two main parts: a continuous radon monitor and an accumulation
233 volume to be placed on the soil surface. The radon flux (or exhalation rate), is then calculated by Eq. 9 using the
234 measured increase of radon within the known volume. However, Eq. 9 can only be solved if the exhalation rate F
235 and the total system leakage λ_{eff} remain constant over the designated time period. This condition is hard to satisfy
236 for long-term radon flux measurements under field conditions, making it difficult to apply the ISO suggested

237 exponential fit. Variability of environmental parameters, in the soil and/or atmosphere, may force changes in the
238 quantity of radon exhaled from the surface. Furthermore, gradients of temperature and/or pressure between internal
239 and external air of the accumulation chamber may increase the leakage of the system. To minimize such problems,
240 it is advisable to perform short radon flux measurements. This is also important when using measurements to
241 validate radon flux models. For short measurement periods, $\lambda_{eff} \cdot t \ll 1$ and the initial concentration within the
242 accumulation chamber is relatively close to the atmospheric value, which is usually small ($C_0 \approx 0$). Thus, Eq. 9
243 can be substituted with a Taylor series of the exponential truncated to the first order as:

$$C_{\mathrm{Rn}}(t) = C_0 e^{-\lambda_{eff} t} + \frac{F \cdot A}{V_{eff} \cdot \lambda_{eff}} \left(1 - e^{-\lambda_{eff} t}\right) \approx \frac{F \cdot A}{V_{eff} \cdot \lambda_{eff}} \cdot \lambda_{eff} t = \frac{F}{h_{eff}} \cdot t = b \cdot t \qquad (10)$$

244

245 where $h_{eff} = V_{eff}/A$ is referred to as the effective height of the system.

246 The main characteristics of radon flux systems in the literature based on continuous radon monitors are
247 summarized here (see Table S3 and Figure S2 of the supplement material for more detail). System 1 was designed
248 and built by ANSTO. While not a commercial system, it is based on a commercial AlphaGUARD (AG) monitor
249 and has a drum-like accumulation chamber with a lid that can be automatically opened and closed. A separate
250 pump is used to circulate air from the accumulation chamber to the AG in a closed loop. No monitoring of the air
251 inside the accumulation chamber is performed by this system. System 2 (the *emanometer*), also designed and built
252 by ANSTO, is the predecessor of the System 1 and is based on the flow-through accumulation method. In this case
253 the accumulation volume is permanently closed and to perform a measurement the edges of the accumulation
254 chamber are buried in soil to make a reasonable seal with the emanating surface (Zahorowski and Whittlestone,
255 1996). The system has two detection volumes (scintillation cells) separated in the flow path by approximatively 5
256 minutes to enable separate radon and thoron (^{220}Rn) flux estimation (more details in Zahorowski and Whittlestone,
257 1996). System 3 is a commercial accumulation chamber designed and built by LI-COR (www.licor.com). To date,
258 this chamber is only sold together with an 8100-401 Chamber Control Kit for the purpose of automatic CO_2 flux
259 measurements. So far it has never been coupled with any commercial radon monitor. Systems 4, 5 and 6 are
260 research products, each using different radon monitors and types of accumulation chambers, some of which can
261 be opened and closed automatically. System 6, in particular, developed at the Helmholtz Zentrum München
262 (Institute of radiation protection), Neuherberg, Germany, allows radon flux measurements to be made at different
263 sites around a circular path, using a mechanical arm (Yang et al., 2017). Unfortunately, system 6 is no longer
264 available due to the discontinuation of the research group. Systems 7 and 8, built by INTE-UPC and UC
265 respectively, are based on radon monitors (DOSEman and AlphaE) operating in diffusion mode. Radon monitors
266 operating in diffusion mode can influence the flux instrument's response time, as well as the subsequent fit
267 calculation for estimating the flux, as will be shown in Section 3. Both systems have accumulation chambers that
268 can only be opened manually, but air is refreshed by an external pump.

269 The importance of the accumulation chamber characteristics when measuring soil gas fluxes should not be
270 underestimated. An inherent challenge in flux chamber design is minimizing the influence that the chamber may
271 have on the measurements, especially for long-term observations. Based on our literature review, the main
272 characteristics required for radon flux systems (monitors and accumulation chambers) are listed and have been
273 taken into account when developing a radon flux system suitable for use as a Transfer Standard.

274 For a system capable of making radon flux measurements at high temporal resolution, which minimizes the
275 disturbance of flux estimates by changing environmental parameters inside the accumulation chamber, the main
276 requirements are:

277   -   to use a continuous radon monitor that measures activity concentration in flow mode (not diffusion mode)
278   at a high temporal resolution (e.g., 1 min - 10 min), and has a minimum detectable radon activity
279   concentration below 100 Bq m^{-3}, allowing radon flux measurements to be obtained using Eq. 10.
280   -   the accumulation chamber needs to open completely and automatically after each measurement period,
281   to establish the initial condition of C_0 equal to the ambient radon concentration.
282   -   environmental sensors are needed inside and outside the accumulation chamber.
283   -   the accumulation chamber needs to have a smooth internal geometry to avoid inhomogeneous internal
284   concentration distribution.
285   -   the accumulation chamber should be painted gloss white, to minimize the temperature difference between
286   air inside and outside of the chamber when the chamber is in direct sunlight.

287   -   the chamber should have a matching collar to attach to (via an easy to clean and seal flange), which can
288   be firmly seated in the soil (to a depth of 2 – 10 cm, depending on soil type / texture) to minimize radon
289   loses (Gutiérrez-Álvarez et al., 2020b).

290

2.5. Design of a new Radon Flux Transfer Standard (TS) System

292

293   Based on the monitor requirements described in section 2.4 an automatic and low maintenance radon flux
294   measurement system was designed and built at ANSTO in September 2020 as an alternative implementation of
295   System 1, described previously. This new system was implemented in collaboration with the UPC, and
296   subsequently fully characterized by UPC in collaboration with UC, in the framework of traceRadon. UPC also
297   implemented the means to remotely control the system for data download during the experiments and improved
298   the scripts for the flux calculations and analysis.

299   This instrument enables 8 automatic flux measurements to be performed each day, every 3 hours. The *AutoFlux* is
300   comprised of an AG PQ2000 PRO (Saphymo) radon monitor (working in 10 min flow mode), an accumulation
301   chamber (drum) with automatic lid, and several environmental sensors installed within the soil, inside the drum,
302   and outside the drum at 50 cm above ground level. An internal lip near the bottom of the accumulation chamber
303   allows the chamber to be pushed 5 cm into the soil to make a good seal with the surface. The radon flux is estimated
304   by performing linear fit of the radon concentration increase within the closed drum every 10 min over a 1 hour
305   period using Eq. 10. The drum's hinged lid is opened and closed using a 150 lb 4" classic rod linear actuator. The
306   actuator is fitted with an external limit switch kit, powered by a 4 x 12V DC relay card and controlled by a CSI
307   CR1000 datalogger (https://www.campbellsci.es/cr1000). The opening (default 2h) and closing (default 1h) times
308   of the accumulation chamber are controlled by the program in the datalogger.

309   The novelty of this system is that the diurnal and seasonal variability of soil radon fluxes can be observed and
310   studied in parallel with measurements of soil properties and meteorological conditions. The *AutoFlux* system was
311   constructed in such a way that it can perform long-term measurements of radon flux and environmental parameters
312   with almost zero maintenance requirements. Unfortunately, this system does not provide a movable arm to allow
313   a periodic change of the measurement spot. Consequently, the positioning of the lid, even when fully open, can
314   sometimes partially shelter the measurement surface from the rainfall that the surrounding surface is receiving. To
315   best match conditions inside and outside of the chamber when open, the accumulation chamber should be
316   positioned such that the lid opens into the direction of the sun at midday, to maximise the sunlight received by the
317   surface inside.

318   Figure 1 shows the *AutoFlux* system during a typical radon flux field measurement. Figure S3 of the supplementary
319   material presents a simplified scheme of the actual state of the *AutoFlux* system.

320

Figure 1. Image of the *AutoFlux* system running in the field. The radon activity concentration, internal air temperature,
differential pressure and soil characteristics are measured within the white drum. Ambient temperature, humidity,

324   **pressure and rainfall are measured on the side of the transport case (~50 cm a.g.l.), and the main system components**
325   **are located inside the waterproof transport case.**

326   The air exhaled from the soil, rich in radon and thoron (^{220}Rn), enters the accumulation volume $V_D = 0.01885$ m^3
327   and is pumped at $Q = (1 \pm 0.1)$ L min^{-1} first through a filter (PALL Acro 50) and then through a Permapure PD
328   gas dryer, intended to maintain humidity levels below saturation conditions within the AG monitor. The low
329   humidity air stream then enters a delay volume ($V_{Th} = 6 \cdot 10^{-3}$ m^3) within which the ambient thoron decays. Next,
330   the air passes into the detection volume of the AG ($V_{AG} = 0.62 \cdot 10^{-3}$ m^3) where the radon concentration is measured
331   with a 10-minute temporal resolution. The total volume of the circuit tubes is $V_{Tubes} \approx 0.3 \cdot 10^{-3}$ m^3. The area of the
332   exhaling surface is $A = 0.126$ m^2. Considering the total volume where the radon concentration will be accumulating
333   V_{eff} will be in this case equal to $V_{tot} = V_D + V_{Th} + V_{AG} + V_{Tubes} = 2.58 \cdot 10^{-3}$ m^3 the effective height h_{eff} in the Eq. 10
334   is equal to 0.204 m.

335   The drum and soil sensors are installed directly into the soil. All sensor outputs are read by a CR1000 datalogger.
336   A Raspberry Pi 4 (RPi) enables scheduled data downloads from both the CR1000 datalogger and AG via a RS232
337   serial port and serial to USB FTDI adapter. The RPi, AG, datalogger, PD and all electronic components of the
338   *AutoFlux* system are safety located within a sturdy, waterproof transport case. External sensors are installed on the
339   outer walls of the blue transport case. Table 1 summarizes the sensors installed within the *AutoFlux* system. Data
340   stored on the RPi, which are downloaded from the AG and datalogger hourly, can be transferred to a notebook
341   computer by connecting the RPi with an Ethernet cable, assuming a Bitvise SSh Client is installed.

342   Figure S4 of the supplementary material shows the accumulation chamber of the *AutoFlux* system in its closed
343   state (left side) and opened state (right side) during a typical radon flux measurement.

344

345

346   **Table 1. Sensors installed within the *AutoFlux* system.**

Variable (Label within the document)	Sensor	Location	Unit (S.I.)	Picture
Volumetric Water Content (VWC) in the soil	CSI CS655 Water Content Reflectometer	Inside Drum	m^3/m^3	
Electrical soil conductivity (EC)	CSI CS655 Water Content Reflectometer	Inside Drum	dS/m	-
Water vapor pressure (VaporPress)	CSI CS655 Water Content Reflectometer	Inside Soil	kPa	-
Soil temperature (T)	CSI CS655 Water Content Reflectometer	Inside Soil	^{0}C	
Drum air temperature (DrumTemp)	SDI-12 sensor Unidata 6508A	Inside Drum	^{0}C	
Atmospheric air Pressure (AtmPress)	Integrated ATMOS-14 sensor	Outside attached to box	mbar	
Ambient air Temperature (AirTemp)	Integrated ATMOS-14 sensor	Outside attached to box	^{0}C	-

Relative Humidity (RH)	Integrated ATMOS-14 sensor	Outside attached to box	%	-
Accumulated rain (Rain)	Hydreon RG-11 Optical Rain Gauge	Outside Drum	mm	
Differential pressure between Drum and external atmosphere (DiffPress)	Novus NP785	Inside/Outside Drum	Pa	

347

2.6. Calibration of a secondary Radon Flux System using the *AutoFlux* and the UC EB facility

349

350 After the characterization of the EB (see Section 3.1), and the calibration of the TS under stable laboratory
351 conditions with a constant reference radon flux (see Section 3.2), they were used together to calibrate a second
352 radon flux system (*INTE_flux*, system 6 of Section 2.3).

353 The *INTE_flux* system also operates continuously and is capable of making 3 radon flux measurements per day. It
354 consists of a cylindrical metallic chamber connected to two electro valves and a pump. The electro valves and
355 pump are controlled using a Programmable Logic Controller (PLC) and the system is powered via a 30 m water-
356 proof cable. To measure a radon flux with this system, the ^{222}Rn concentration in the chamber exhaled from the
357 soil surface is continuously measured using a DOSEman monitor in diffusion mode, which was previously
358 calibrated at the Radon Reference Chamber (secondary) of the INTE-UPC in agreement with the IEC 61577-4.
359 The DOSEman monitor is powered by an internal battery that lasts 15 days.

360 A typical calibration experiment setup, as carried out at the UC EB facility, is shown in Figure 2, where the
361 *INTE_Flux* and TS were installed on the EB between the 29th of June 2021 and 1st of July 2021.

362

Figure 2. Typical calibration experiment carried out at the UC laboratory: the *INTE_Flux* system is installed together with the TS system on the EB facility.

365

3 Results

367

3.1. Characterization of the Radon Exhalation Bed (EB) facility

369

370 The EB radon flux was determined under laboratory conditions at specific points in time using both theoretical
371 and experimental approaches, as explained in Section 2.1. The necessary parameters to apply Eq. 3 were measured
372 and/or calculated as explained later in this section and are presented in Table 2, along with their respective

373 uncertainties (with k=1). Table 2 also presents all variables and parameters measured or calculated for the
374 experimental characterization of the EB within a week of its installation, together with values obtained from the
375 literature (D and λ).

3.1.1 Radium activity concentration (C_{Ra})

376
377

378 The average radium activity concentration of the soil in the EB was obtained by gamma spectrometry analysis of
379 5 separate samples. The samples were extracted from the center and each of the four corners of the EB at a depth
380 of 10-15 cm. Samples were hermetically sealed in a cylindrical container for one month to allow equilibrium to be
381 reached between radon progeny and the radium activity concentrations, after which time the radium activity was
382 determined in a high-resolution gamma HPGe coaxial detector (model GL-2015-7500, Canberra, USA) following
383 Celaya et al., (2018). The mean ^{226}Ra activity concentration was 19130 ± 350 Bq kg^{-1}.

3.1.2 Emanation factor (ε)

384
385

386 The emanation factor, ε, of the EB soil was obtained from the soil radium activity concentration and the radon that
387 escapes to the pore spaces (Eq. 2). The radon activity in a $M = 100$ g soil sample was measured, hermetically
388 sealing it within a volume $V = 0.024$ m^3 and making an exponential approximation of the radon concentration
389 increase with time according to Eq. 9. To facilitate radon escape to the air volume, the soil sample was distributed
390 in a layer less than 5 mm thick.

391 The experiment was run over a period of 500 hours and was replicated in three identical boxes to evaluate the
392 uncertainty of ε. The continuous radon monitor (Radon Scout; Sarad GmbH) used for these tests was calibrated
393 in the LaRUC radon chamber (Fuente et al., 2018). A final emanation factor of 0.18 ± 0.03 was obtained as:

$$\varepsilon = \frac{A_{\text{Rn}}}{A_{\text{Ra}}} = \frac{\phi}{\lambda_{eff} \cdot C_{Ra} \cdot M} = \frac{0.032 \cdot 0.024}{2.2 \cdot 10^{-6} \cdot 19130 \cdot 0.1} = 0.18 \tag{11}$$

394

395 with ϕ the activity rate of radon (Bq s^{-1}) and $\lambda_{eff} = (2.2 \pm 0.3) \cdot 10^{-6}$ s^{-1}, the effective decay constant of the system.
396 It can be observed that $\lambda_{eff} \approx \lambda$. A typical measurement result is shown in Figure S6 of the supplementary material.

397 As mentioned in the introduction, the emanation factor is not constant over time because – apart from the grain
398 size – it also depends on the moisture content and temperature of the material. Zhuo et al., (2006) and Zhuo et al.,
399 (2008) investigated the relationship between the emanation factor variability with soil moisture and soil
400 temperature, and derived the following empirical relationship Eq. 12:

$$\varepsilon = \varepsilon_0 \cdot [1 + a(1 - e^{-bw_s}))] \cdot [1 + c(T - 298)] \tag{12}$$

401

402 where ε is the radon emanation factor estimated for a given temperature T, and ε_0 is the radon emanation factor
403 measured at a temperature of $T = 298$ K for dried soil. w_s is the water saturation fraction and a, b, c are parameters
404 calculated for different types of soil textures and declared by Zhuo et al., (2008).

3.1.3 Bulk density (ρ)

405
406

407 The soil bulk density ρ was calculated by measuring the mass, M, with a calibrated balance, and dividing this by
408 its volume, V_s. The volume was measured from an undisturbed soil sample using a test tube manufactured
409 according to ISO 4788. A value of 1645 ± 2 kg m^{-3} was calculated.

3.1.4 Radon diffusion length (L)

410

411 As explained in Section 2, to simplify Eq. 1 to Eq. 3 the soil thickness z of the EB needs to be much smaller than
412 the radon diffusion length L in the material. Equations 4 to 7 had to be applied after measuring and/or calculating
413 the required soil parameters for these equations: water saturation (w_s) and porosity (p) of the soil. In addition, to
414 apply Eq. 6 and 7 the grain density and water content of the soil sample had to be measured. The mass water
415 content w_c (kg/kg) can be measured as the ratio of the mass of water and the mass of dry soil. It is measured by
416 weighing a soil sample, m_{wet}, then drying the sample to remove the water and weighing it again, m$_{dry}$:

$$w_c = \frac{m_{wet} - m_{dry}}{m_{dry}} \tag{13}$$

417 The grain density ρ_g is the ratio of the mass of a dry sample and its volume after eliminating the contribution of
418 the interparticulate void volume. It can be calculated from the sample weight m_{dry} and the volume V_{dry} of dry soil
419 from:

$$\rho_g = \frac{m_{dry}}{V_{dry}} \qquad (14)$$

420

421 The diffusion coefficient D and the diffusion length L can now be calculated using Eq. 4 and 5 and L is equal to
422 (1.286 ± 0.015) m. The measured EB thickness is equal to (0.165 ± 0.005) m, thus the hypothesis $z << L$ is verified.
423 Using all the previous parameters the radon flux from the EB can be theoretically estimated by Eq. 3 and it is
424 $F_{Th\_EB} = 1918 \pm 278$ mBq m^{-2} s^{-1}.

425 Figure 3 shows the theoretical radon flux of the EB calculated using Eq. 1 assuming that the emanation factor
426 varies according to Eq. 11 of Zhuo et al., (2008). The two versions of radon flux presented in Figure 3 represent
427 changes in the adopted diffusion coefficient D. In one case the flux has been calculated using D from Eq. 5 (blue
428 dots) and the other, D from Eq. 5a (black dots). It is evident that no significant difference in EB flux estimate was
429 observed between these methods in the range of water saturation values for which the EB characterization was
430 performed.
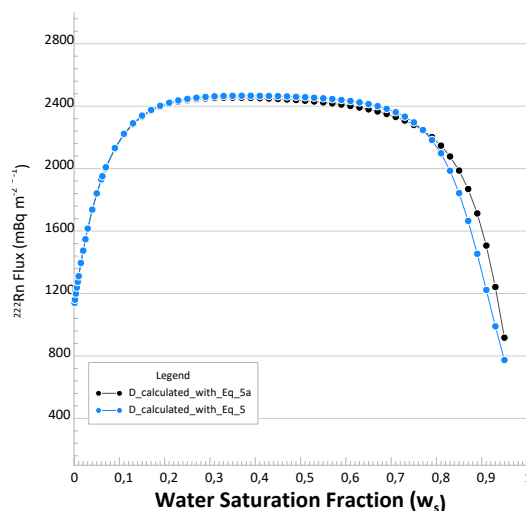
431

432 **Figure 3. Variability of EB ^{222}Rn flux calculated using Eq. 1 where the emanation factor variability follows Eq. 11 and**
433 **the diffusion coefficient D was estimated using both Eq. 5 (black dots) and Eq. 5a (blue dots).**

434

435 As explained in the Methods section, an empirical evaluation of the EB radon flux was also undertaken by
436 enclosing the whole exhaling surface with a cover of known volume. The experiments were performed using
437 different radon monitors inside the closed volume to monitor the radon buildup. Figure S5 of the supplementary
438 material shows the results of a typical accumulation experiment to estimate the EB radon exhalation rate. The
439 experiment was repeated several times. The response time of the RTM device was set to 1 minute, while it was 10
440 minutes for the Radon Scout and AlphaE. Air samples were also collected from the enclosed volume every 15
441 minutes for independent analysis. Radon concentrations inside the volume reached values of about 130 kBq m^{-3}
442 after only 5 hours. The diffusion mode of operation for the AlphaE and Radon Scout monitors (green and orange
443 dots, respectively in Figure S6) is not capable of correctly representing the temporal variability of radon within
444 the volume, so data from these devices were not used to estimate the EB radon exhalation rate.

445

446 The radon exhalation rate was calculated according to Eq. 10, using calculated or measured values and parameters
447 summarised in Table 2. Mean values reported by the environmental sensors of the EB facility are also reported.
448 The resulting empirical flux estimate was $F_{exp\_EB} = 1757 \pm 67$ mBq m^{-2} s^{-1}.

449

Table 2. Results of the parameters influencing the calculation of radon flux from the Exhalation Bed configuration for the theoretical and experimental approaches. Uncertainties are expressed without any coverage factor (k=1).

Parameter	Symbol	Result
Emanation factor	ε	0.18 ± 0.03
Radium concentration	C_{Ra}	(19130 ± 350) Bq kg^{-1}
Bulk density	ρ	(1645 ± 2) kg m^{-3}
Grain density	ρ_g	(2570 ± 38) kg m^{-3}
Thickness	z	(0.165 ± 0.005) m
Mass Water content	w_c	(0.0132 ± 0.0004) kg/kg
Water saturation	w_s	(0.061 ± 0.008) m^3/m^3
Porosity	p	0.3599 ± 0.0001
Diffusion coefficient	D	$(3.47 \pm 0.08) \cdot 10^{-6}$ m^2/s
Diffusion length	L	(1.286 ± 0.015) m
Radon decay constant	λ	$2.0993(1) \cdot 10^{-6}$ s^{-1}
^{222}Rn *Flux*	$F_{Th\_EB} \pm u_{Th\_EB}$	1918 ± 278 mBq m^{-2} s^{-1}
Parameter/Variable	**Symbol**	**Result**
Radon emission rate	ϕ	(7.78 ± 0.29) Bq s^{-1}
Height of Chamber	h	(0.225 ± 0.005) m
Air temperature	T	(20.7 ± 0.3) °C
Mass water content in mass	w_c	(0.013 ± 0.001) kg/kg
Air moisture	RH	(47.0 ± 0.7)%
^{222}**Rn Flux**	$F_{Exp\_EB} \pm u_{Exp\_EB}$	1757 ± 67 mBq m^{-2} s^{-1}

452

3.2 Characterization of the Radon Flux Transfer Standard (TS) System

454

The *AutoFlux* was characterized and calibrated under controlled laboratory conditions using the EB facility as described previously. Figure S7 of the supplementary material shows the *AutoFlux* setup for a typical laboratory measurement at UC. Two laboratory experiments were performed at standard environmental conditions: i) from the 28th of June 2021 to the 1st of July 2021 (19 radon flux measurements); and ii) from the 7th to the 12th of July 2021 (39 radon flux measurements). Figure 4 shows the radon activity concentrations (upper panels) measured by the *AutoFlux*'s AG during the two continuous experiment periods for each accumulation hour. The bottom panels of Figure 4 show the soil Volume Water Content (*VWC*) time series measured by the CSI CS655 Water Content Reflectometer and the air temperature inside the drum measured by the SDI-12 (Unidata 6508A) sensor during these experiments. A constant increase of around $28 \cdot 10^3$ Bq m^{-3} of radon and of 1 °C of temperature was measured during the 1 h accumulation phase within the system. The Volume Water Content (VWC) measured during the two experiments ranged between 0.025 m^3/m^3 and 0.029 m^3/m^3.

466

467
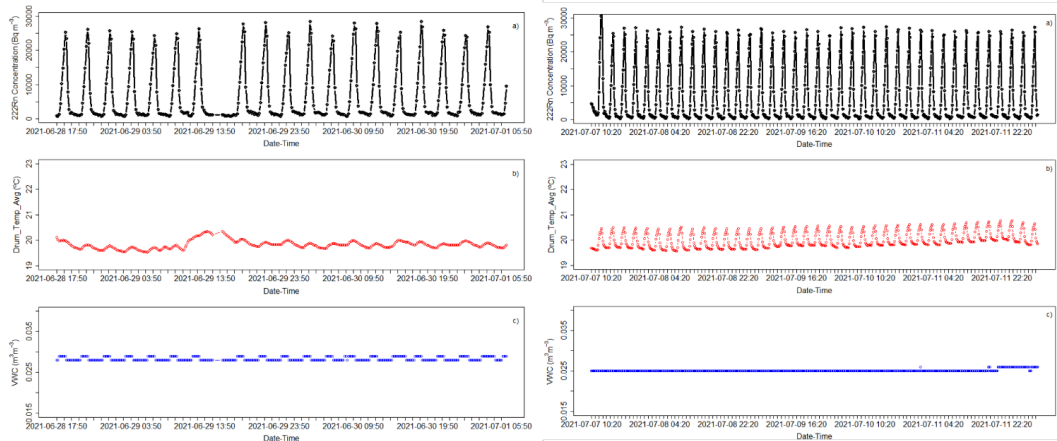
Figure 4. Radon activity concentrations (black dotted lines in panel *a*) measured by the *AutoFlux*'s AG during the two calibration experiments. The bottom panels show the time series of the soil *VWC* (blue dotted lines in panel *c*) and air temperature inside the drum (red dotted lines in panel *b*) during the experiments.

An example of the increase in radon activity concentration measured by the *AutoFlux*'s AG during a typical 1h accumulation period for a single flux measurement is shown in Figure 5. It is evident that the first two values after the chamber closes (0 and 1 in Fig. 5) do not follow the expected theoretical linear increase from Eq. 10. Including these values in the slope calculation could lead to an underestimation of the flux. To better understand the process going on within the drum during a measurement, it is important to note that the 10-minute AG data are representative of the mean radon activity concentration measured over that period, and that the timestamp assigned to each recorded value is at the end of each measurement period. Consequently, the first output value after the chamber is closed (0 in Fig. 5) actually represents the mean radon concentration measured over the 10-minute period leading up to the point of closure. This value has therefore not been considered for the experimental linear fit analysis.

A box model (Eq. 15, 16 and 17 and Figure S8 of the supplementary material) can be used to better understand the behavior of radon activity concentrations in the *AutoFlux* system. Figure S8 shows the three main volumes of the system: V_{AG} is the AlphaGUARD detection volume; V_D is the drum (accumulation chamber) volume and V_u is the total volume of all tubing (V_{tubes}) plus the thoron delay volume (V_{Th}). The change in radon concentration with time in each volume of the system components can be described by the following set of differential Equations:

$$\frac{dC_D(t)}{dt} = \frac{F \cdot A}{V_D} - C_D(t) \cdot \frac{Q}{V_D} + C_{AG}(t) \cdot \frac{Q}{V_{AG}} \tag{15}$$

$$\frac{dC_u(t)}{dt} = C_D(t) \cdot \frac{Q}{V_D} + C_u(t) \cdot \frac{Q}{V_u} \tag{16}$$

$$\frac{dC_{AG}(t)}{dt} = C_u(t) \cdot \frac{Q}{V_u} + C_{AG}(t) \cdot \frac{Q}{V_{AG}} \tag{17}$$

Figure S9 of the supplementary material shows the theoretical increase of radon concentration with time in each of the respective volumes C_D (drum concentration), C_u (concentration in thoron delay and tubes) and C_{AG} (concentration in the AG) during the first hour of system closure, obtained through the analytical solution of Eq. 15, 16 and 17 with the software Mathematica (Wolfram Mathematica). The observed increase in radon within the AG becomes parallel to the radon increase within the accumulation chamber only after 700 sec ($\approx$ 12 minutes). Therefore, the second value measured by the AG after the accumulation volume is closed (point 1 in Figure 5) also can't be considered as part of the experimental linear fit analysis due to the system response time delay.

Looking at Figure 5, the slope of the experimental data (black dotted line) during the accumulation hour, ignoring the first two points (0 and 1) for the reasons mentioned above, gives a radon flux of (1899 ± 60) mBq m^{-2} s^{-1} according to Eq. 10, where the associated uncertainty is calculated from the residual standard error (rse) of the linear fit. These data were measured with a mean volume water content w_V of 0.025 m^3/m^3, equal to a soil water saturation $w_s = 0.069$ m^3/m^3 that, according to Eq. 1 and 11, gives a theoretical radon flux of (1974 ± 277) mBq m^{-2} s^{-1}. Finally, the theoretical data (blue dotted line) obtained by solving differential equations 15, 16 and 17 were calculated with a radon flux of about $(F_{Th\_AF} = 1871 \pm 187)$ mBq m^{-2} s^{-1} where the uncertainty of 10% (k=1) is due to the volume estimations and flow variability during the accumulation hour. All of these results are consistent if the associated uncertainties are taken into account and support the understanding of the system response.

Radon concentration time series obtained by exposing the *AutoFlux* system to the UC EB facility (Experiments I and II in Figure 4) were analyzed and Eq. 10 was used to calculate the radon fluxes for each measurement, using only points 2, 3, 4, 5 and 6 of the accumulation phase. This resulted in a mean radon flux of $F_{Exp\_AF} = 1856$ mBq m^{-2} s^{-1} with a standard deviation of $\sigma_{Autoflux} = 86.5$ mBq m^{-2} s^{-1} over a total of n = 58 radon flux measurements. The error of the mean of the flux measured experimentally by the *Autoflux* monitor will be $u_{Autoflux} = \frac{\sigma_{Autoflux}}{\sqrt{n}} = 11.4$ mBq m^{-2} s^{-1}. All results are consistent within their respective uncertainties. Finally, Table 3 summarizes the mean radon flux measured by the *AutoFlux* system during experiments I and II at the UC EB facility in October 2021. The means and standard deviations of the variables measured by the *AutoFlux* environmental sensors are also reported.

Table 3. Results of ^{222}Rn fluxes and environmental parameters calculated and/or measured using the *AutoFlux* system during experiments I and II carried out at the UC facility in October 2021 (Grey shaded values have been calculated using Eq. 10 and 15-16-17).

Variable	Mean	St. Dev.
F_{Exp_AF} (mBq m^{-2} s^{-1})	1856	86.5
F_{Th_AF} (mBq m^{-2} s^{-1})	1871	187
Flow (L min^{-1})	0.91	0.01
VWC (m^3/m^3)	0.025	0.002
AirTemp (^{0}C)	19.92	0.095
RH (%)	69.91	1.58
AtmPress (mbar)	1015.3	2.5
DrumTemp (^{0}C)	20.04	0.11
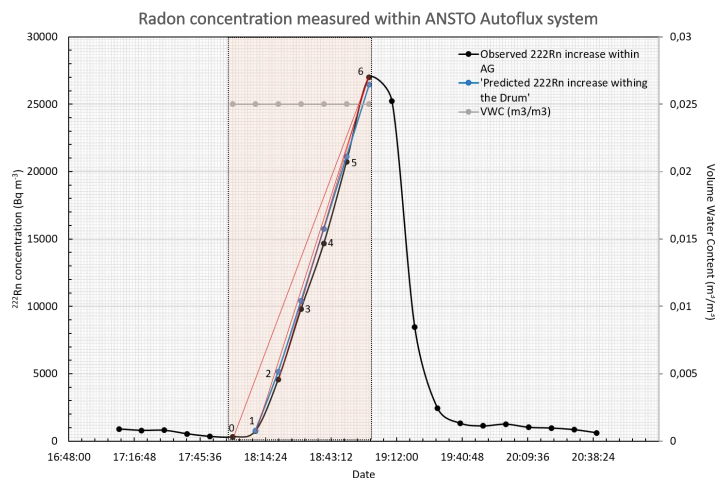
Figure 5. Increase in radon activity concentration within the *Autoflux's* accumulation chamber during a typical radon flux measurement (black dotted line). Blue dotted line represents the theoretical value calculated within the AG volume. The grey dots indicate the *VWC* measured in the soil at the same time. Red lines show different slopes obtained when considering different values.

526

527 Considering the agreement between the theoretical and experimental results of the mean radon flux values obtained
528 directly from the EB (F_{Th_EB} and F_{Exp_EB}) or using the *Autoflux* on the EB (F_{Th_AF} and F_{Exp_AF}), the calibration factor
529 of the *AutoFlux* monitor can be now calculated as $F_{Cal\_Autoflux} = F_{Exp\_EB}/F_{Exp\_AF} = 0.95$. The uncertainty of the
530 calibration factor $u_{Cal\_Autoflux} = 0.07$, calculated following the 'Guide to the Expression of Uncertainty in
531 Measurement' (JCGM 100) by Eq. 18:

532
$$\left(\frac{u_{Cal\_Autoflux}}{F_{Cal\_Autoflux}}\right)^2 = \left(\frac{u_{Autoflux}}{F_{Autoflux}}\right)^2 + \left(\frac{u_{Exp\_EB}}{F_{Exp\_EB}}\right)^2 + \left(\frac{u_{F\_Corr}}{F_{Corr}}\right)^2 \quad (18)$$

533 It should be noted that F_{Exp_EB} and F_{Exp_AF} were measured within a 1% of variability of the water saturation
534 condition of the emanating soil, which could induce up to a 6% of variability on the measured flux. This possible
535 variability should be considered within the calculation of the uncertainty of the calibration factor of the Transfer
536 Standard monitor, including a correction factor $F_{Corr} = 1$ with un uncertainty $u_{F\_Corr} = 0.06$.

537

538 **3.3. Calibration of the INTE_Flux system using the TS and the EB facility**
539

540 The upper panel of Figure 6 shows the radon concentration time series measured at the same time by the DOSEman
541 included within the accumulation chamber of the *INTE_Flux* system and by the AG used for the *AutoFlux* system.
542 The slope b in Eq. 10 can be calculated for each radon accumulation period of the *INTE_Flux* and it has been
543 reported in Table 4, together with the radon fluxes measured by the *INTE_Flux* when a nominal $h_{eff} = 0.15$ m is
544 applied. The mean value of the radon flux calculated using the *INTE_Flux* system was $F_{Client} = 1332$ mBq m^{-2} s^{-1}
545 with a standard deviation of $\sigma_{Client} = 140$ mBq m^{-2} s^{-1} and the standard error of the mean $u_{Client} = \frac{\sigma_{Client}}{\sqrt{n}} = 63$ mBq
546 m^{-2} s^{-1}, where n = 5, the number of radon flux measurements carried out with the *INTE_Flux* system. The mean of
547 the radon flux measured by the TS instrument (*AutoFlux*) during the same period was $F_{Ref} = 1868$ mBq m^{-2} s^{-1} with
548 a standard deviation of $\sigma_{Ref} = 137$ mBq m^{-2} s^{-1} and a standard error of the mean $u_{Ref} = 39.5$ mBq m^{-2} s^{-1} ($n_{Ref} = 12$).
549 The calibration factor of the *INTE_Flux* system can be estimated as $F_{Cal} = F_{Ref\_Cal}/F_{Client} = 1.33$, where $F_{Ref\_Cal} =$
550 $F_{Ref} \cdot F_{Cal\_Autoflux}$ represents the calibrated radon flux value obtained by the ANSTO *Autoflux* system over the
551 experiment.

552

553

554
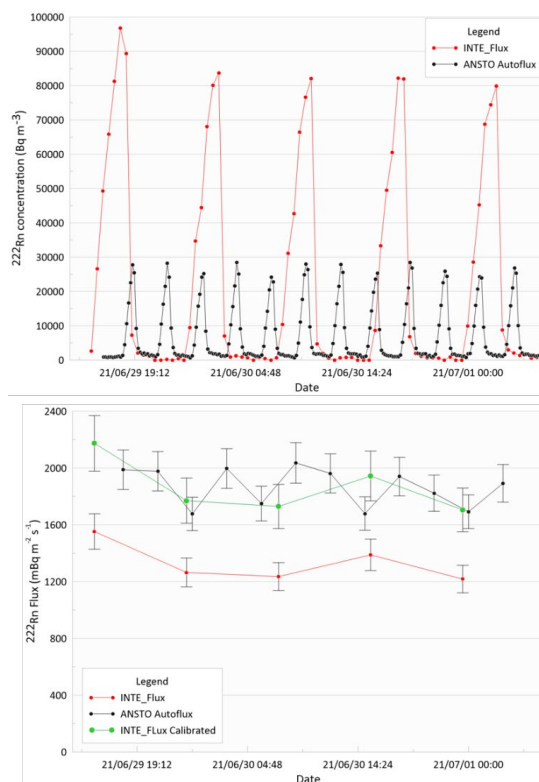
Figure 6. Upper Panel: Time series of radon concentrations measured by the DOSEman (output each 30 min) in the *INTE_Flux* system accumulation chamber and by the AG (output each 10 min) used for the *AutoFlux* on the EB facility of the Cantabria University during the accumulation and ventilation phases of both instruments. Lower panel: Time series of the radon fluxes obtained with the *AutoFlux* system (black dotted line), by the *INTE_Flux* system (*Client*) before the calibration factor being applied (red dotted line) and after its application (green dotted line).

Table 4. Slope and Fluxes obtained by Eq. 10 for the *INTE_Flux* system.

Slope b (Bq m^{-3} h^{-1})	F_{Client} (mBq m^{-2} s^{-1})
37239	1553
30325	1265
29629	1235
33301	1389
29209	1218
Mean ± Standard Deviation	
(1332 ± 140) mBq m^{-2} s^{-1}	

To estimate the total uncertainty (u_{cal}) of the calibration factor F_{Cal} in agreement with the 'Guide to the Expression of Uncertainty in Measurement' (JCGM 100) was used Eq. 19:

$$\left(\frac{u_{Cal}}{F_{Cal}}\right)^2 = \left(\frac{u_{Client}}{F_{Client}}\right)^2 + \left(\frac{u_{ref}}{F_{ref}}\right)^2 + \left(\frac{u_{Cal\_Autoflux}}{F_{Cal\_Autoflux}}\right)^2 \qquad (19)$$

568 Thus, the calibration factor F_{Cal} value will be obtained with a total associated uncertainty equal to $u_{Cal} = 0.12$ which
569 corresponds to 9% of the calibration factor. To ensure a confidence level of 95% the Welch–Satterthwaite equation
570 was used to calculate an approximation to the effective degrees of freedom of the u_{cal} variable and to select the
571 corresponding t-student coverage factor. A total expanded uncertainty $U_{cal} = 0.24$ (k=2) was calculated.

572

573 **3.4 Short field comparison between TS, *INTE_Flux* and modeled radon fluxes**

574

575 The calibrated *Autoflux* and *INTE_Flux* systems were used during two intercomparison campaigns presented by
576 Rabago et al., 2022. Figure 7 shows time series of radon concentrations measured within both systems at a low
577 radium content area campaign between the 23rd and the 28th of October, 2021 in Esles de Cayón, Spain (lat.: 43.28,
578 long.: -3.80). Time series of measured VWC and drum temperature from the *Autoflux* are also shown. It can be
579 noted that temperature cycles are mostly related with day/night atmospheric condition where the soil moisture
580 shows a generally decreasing trend over the duration of the campaign. The reader should take into account that the
581 higher radon concentrations measured by the *INTE_Flux* system are inversely proportional to its smaller volume.

582
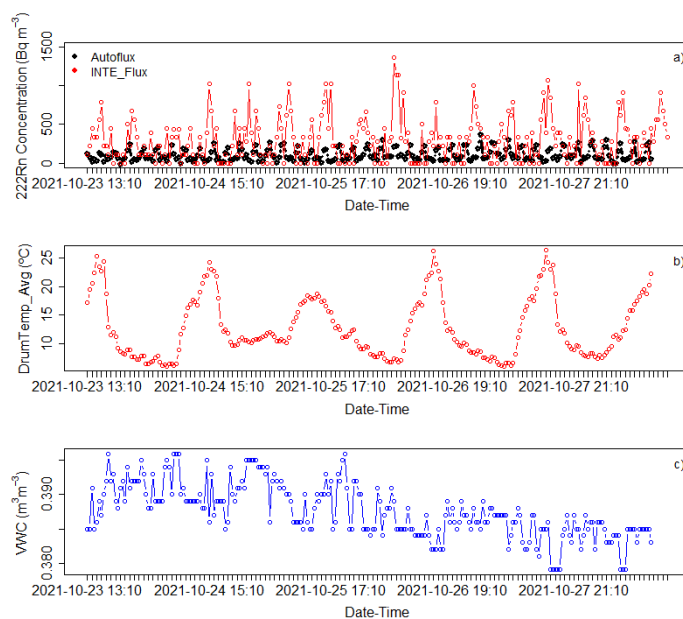
583

584

585 **Figure 7. (a) Time series of radon concentrations measured by the *Autoflux's* AG every 10 minutes (black dotted line)**
586 **and the *INTE_Flux's* DOSEman every 30 minutes (red dotted line), (b) drum temperature (red dotted line), and (c)**
587 **VWC (black dotted line) measured by *Autoflux* sensors.**

588 Daily mean radon fluxes measured by the *Autoflux* and *INTE_Flux* systems throughout the campaign are shown
589 in Figure 8c together with:

590   i)   Data from the traceRadon daily radon flux maps for Europe 2021 (Figure 8a) based on ERA5-Land
591   and on GLDAS-Noah v2.1 soil moisture reanalysis data (Figure 8b), respectively, available at the
592   ICOS Carbon Portal (Karstens, U. and Levin, I., 2022). Radon fluxes are calculated following
593   Karstens et al., 2015 and including the calculation of the emanation factor proposed by Zhuo et al.,
594   2008 but taking into account only half of the temperature influence (c/2 in Eq. 12). The soil uranium
595   content and the soil proprieties needed to apply Eq. 1 within these maps were extracted by EANR,
596   2019 and ESDB, Hiederer, 2013, respectively.

597   ii)   Radon fluxes calculated applying the model by Karstens et al., 2015 and the complete emanation
598   factor proposed by Zhuo et al., 2008 with soil temperature and soil moisture values measured by
599   *Autoflux* sensors during the measurement campaign. Uranium content of the soil and soil parameters
600   to apply Eq. 1 were directly measured in the laboratory on soil samples extracted at the measurement
601   site.

603 It can be observed that radon fluxes measured by the two calibrated systems are in agreement during the field
604 measurements and they increase throughout the campaign in accordance with the decrease in soil water content
605 (Figure 7c). Output of the model based on ERA5_Land data does not show any increase over the measurement
606 period but they are in agreement with the observed data. Radon fluxes modeled using GLDAS_Noah reanalysis
607 data or local measured parameters seem to be twice as high as other values. This might be related to an
608 underestimation of the soil water saturation data by the *Autoflux* or by GLDAS_Noah for these days.

609
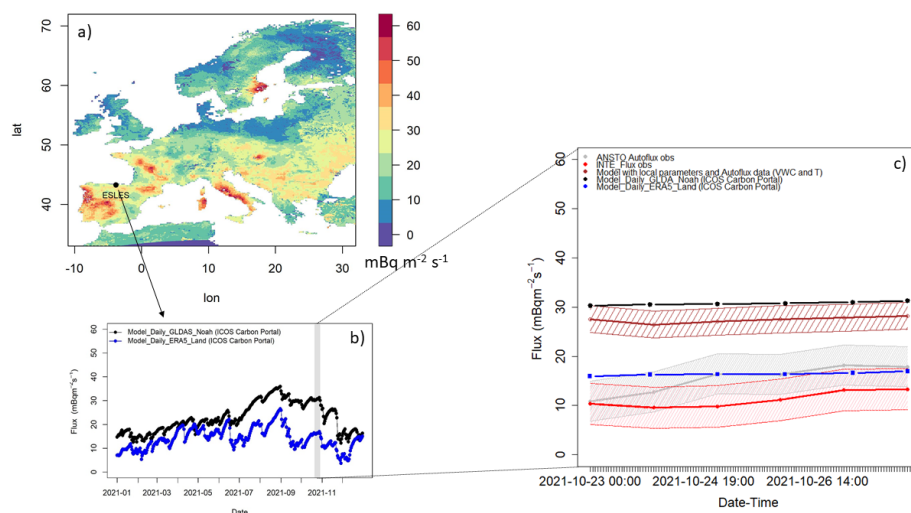
610

611 **Figure 8. a) Radon flux map for Europe for October 2021 based on GDAS_Noah reanalysis data and Esles location; b)**
612 **Time series of daily radon fluxes for 2021 modeled using GLDAS_Noah (black dots) and ERA5_Land (Blue dots)**
613 **reanalysis data at Esles coordinates; c) Daily fluxes and standard deviations of: *Autoflux* observations (black dotted**
614 **line), *INTE_Flux* observations (red dotted line), model based on measurements (brown dotted line), model based on**
615 **ERA5_Land reanalysis (orange dotted line) and GLDAS_Noah reanalysis (blue dotted line).**

616

617 **Conclusions**
618

619 Reliable long-term radon flux observations are important to validate radon flux maps used for radiation protection
620 and climate proposes.

621 In the present study a new automatic radon flux system, which allows 3-hourly measurement of radon fluxes
622 together with environmental parameters in the soil and ambient air, has been characterized and calibrated for be
623 used as Transfer Standard to enable traceable radon flux measurements. This was done using a bespoke exhalation
624 bed built and characterized for this purpose. The new radon flux system (*Autoflux*) was then used to calibrate a
625 second radon flux monitor (*INTE_Flux*). Both calibrated monitors were tested during a short in situ measurement
626 campaign and results were compared with ones obtained from available radon flux maps using soil proprieties
627 from European datasets (traceRadon daily radon flux maps for Europe 2021 based on ERA5-Land and on GLDAS-
628 Noah v2.1 soil moisture reanalysis data, respectively, available at the ICOS Carbon Portal) or local measurements.

629 Based on the results so far, the *AutoFlux* system appears to be a reasonable option for a Transfer Standard, however
630 further studies of this kind should be carried out at lower reference radon exhalation rates (in the order of tens mBq
631 m^{-2} s^{-1}) and under extreme environmental conditions of soil moisture and temperature to better understand sub
632 daily timescale variability of measured fluxes.

633 Daily radon flux observations during the short field intercomparison campaign carried out in northern Spain from
634 the two calibrated systems are coherent, within their daily standard deviations, and in agreement with the daily
635 radon fluxes modeled using ER5_Land reanalysis. Daily radon fluxes modeled using local measured parameters
636 and variable or GDAS_Noah reanalysis data show higher values. This last result shows the importance to validate
637 the input parameters (porosity, bulk density, etc.) and variable (i.e. volume water content and temperature in the
638 soil) used within the model and to perform long-term measurements at different soils and under different
639 meteorological conditions.

640 **Author Contributions**
641

642 C. Grossi, D. Rabago, S. Chambers, R. Curcoll and A. Vargas led the data analysis and the writing of the
643 manuscript. D. Rabago, C. Sáinz and L. Quindos carried out the literature study and the design, building and
644 characterization of the Exhalation Bed facility. P.PS. Otáhale and E. Fialová led the literature study of the radon
645 flux systems. C. Grossi, A. Vargas and D. Rabago carried out the experimental and theoretical characterization of
646 the *Autoflux* system. All authors participated in the discussion of the results and the writing of the manuscript.

647

648 **Acknowledgments**

649 Authors declare do not have any conflict of interest.

650 This study has been possible thanks to the project 19ENV01 traceRadon. The project 19ENV01 traceRadon has
651 received funding from the EMPIR programme co-financed by the Participating States and from the European
652 Union's Horizon 2020 research and innovation programme. 19ENV01 traceRadon denotes the EMPIR project
653 reference.

654 Authors want to thank the work of Sylvester Werczynski, previously employed at ANSTO, who worked on the
655 design and control software of the *Autoflux* system and of Ute Kartsens who made available the radon fluxes
656 model data.

657 **Code and data availability**

658 The data and the codes from this study are available from the corresponding author and at the following link:
659 https://github.com/ClauGro/GRL_Data. Scripts of the software R v. 3.6.2 (with Rstudio) and Phyton v. 3.8 (with
660 Spyder) were used and are also shared in the github repository.

661

662 **References**

663

664 Altic, N. A. (2014). *Pilot study report for radon exhalation measurements*. Oak Ridge Associated
665 Universities, Tennessee.

666
667 Baskaran, M. (2016). *Radon: A tracer for geological, geophysical and geochemical studies*. Springer. Detroit
668 (USA). doi: 10.1007/978-3-319-21329-3.

669
670 Chambers, S.D. Williams, A.G. Conen, F. Griffiths, A.D. Reimann, S. Steinbacher, M. Krummel, P.B. Steele,
671 L.P. van der Schoot, M.V. Galbally, I.E. Molloy, S.B. Barnes, J.E. (2015): Towards a universal "baseline"
672 characterisation of air masses for high- and low-altitude observing stations using Radon-222, Aerosol and Air
673 Quality Research 16, 885–899, doi: 10.4209/aaqr.2015.06.0391.

674
675 Chambers SD, Preunkert S, Weller R, Hong S-B, Humphries RS, Tositti L, Angot H, Legrand M, Williams
676 AG, Griffiths AD, Crawford J, Simmons J, Choi TJ, Krummel PB, Molloy S, Loh Z, Galbally I, Wilson S,
677 Magand O, Sprovieri F, Pirrone N and Dommergue A. (2018): Characterizing Atmospheric Transport

Pathways to Antarctica and the Remote Southern Ocean Using Radon-222, Front. Earth Sci., 6:190, doi: 10.3389/feart.2018.00190.

Ferry C., Beneito A., Richon P. and Robe M.-C. (2001): An Automatic Device for Measuring the Effect of Meteorological Factors on Radon-222 Flux from Soils on the Long-term, *Radiation Protection Dosimetry*, Volume 93, Issue 3, 1 February 2001, Pages 271–274, doi: 10.1093/oxfordjournals.rpd.a006439.

Grossi C., Vargas A., Camacho A., Lopez C. I., Bolívar J., Xia Y. and Conen F. (2011): Inter-Comparison of Different Direct and Indirect Methods to Determine Radon Flux from Soil. Radiation Measurements. 46. 112-118, doi: 10.1016/J.Radmeas.2010.07.021.

Grossi, C., Vogel, F. R., Curcoll, R., Àgueda, A., Vargas, A., Rodó, X., and Morguí, J.-A. (2018): Study of the daily and seasonal atmospheric CH_4 mixing ratio variability in a rural Spanish region using ^{222}Rn tracer, Atmos. Chem. Phys., 18, 5847–5860, doi: 10.5194/acp-18-5847-2018.

Gutiérrez-Álvarez, I., Martín, J. E., Adame, J. A., Grossi, C., Vargas, A., & Bolívar, J. P. (2020a). Applicability of the closed-circuit accumulation chamber technique to measure radon surface exhalation rate under laboratory conditions. *Radiation Measurements*, *133*, 106284, doi: 10.1016/j.radmeas.2020.106284.

Gutiérrez-Álvarez, I., Guerrero, J. L., Martín, J. E., Adame, J. A., & Bolívar, J. P. (2020b). Influence of the accumulation chamber insertion depth to measure surface radon exhalation rates. Journal of hazardous materials, 393, 122344, doi: 10.1016/j.jhazmat.2020.122344.

Hassan, N. M., Hosoda, M., Ishikawa, T., Sorimachi, A., Sahoo, S. K., Tokonami, S., and Fukushi, M. (2009). Radon migration process and its influence factors; review. Japanese Journal of Health Physics, 44(2), 218-231, doi: 10.5453/jhps.44.218.

Hosoda, M., Shimo, M., Sugino, M., Furukawa, M., & Fukushi, M. (2007). Effect of soil moisture content on radon and thoron exhalation. Journal of nuclear science and technology, 44(4), 664-672, doi: 10.1080/18811248.2007.9711855.

IAEA (2004). Soil Sampling for Environmental Contaminants, IAEA-TECDOC-1415, IAEA, Vienna.

IAEA (2013). Measurement and Calculation of Radon Releases from NORM Residues, IAEA-TECDOC-77, IAEA, Vienna.

Indoria, A. K., Sharma, K. L., & Reddy, K. S. (2020). Hydraulic properties of soil under warming climate. Climate Change and Soil Interactions, 473-508, doi: 10.1016/B978-0-12-818032-7.00018-7.

ISO (2009). ISO 61577-7:2009. Equipment for the production of reference atmospheres containing radon isotopes and their decay products (STAR). ISO: Geneva, Switzerland.

ISO/IEC (2015) 13528:2015. Statistical methods for use in proficiency testing by interlaboratory comparison.
Jin, Y. and Jury, W. A. (1996): Characterizing the Dependence of Gas Diffusion Coefficient on Soil Properties, Soil Sci. Soc. Am. J., 60, 66–71, doi: 10.2136/sssaj1996.03615995006000010012x.

Karstens, U., Schwingshackl, C., Schmithüsen, D., and Levin, I. (2015): A process-based ^{222}radon flux map for Europe and its comparison to long-term observations, Atmos. Chem. Phys., 15, 12845–12865, doi: 10.5194/acp-15-12845-2015.

Karstens, U. and Levin, I., 2022. traceRadon daily radon flux map for Europe 2021 (based on ERA5-Land soil moisture), https://hdl.handle.net/11676/NvC7D-BVXlnHtFBdUSKpNVHT, Access Date: 22nd August, 2022.

Karstens, U. and Levin, I., 2022b. traceRadon daily radon flux map for Europe 2021 (based on GLDAS-Noah v2.1 soil moisture), https://hdl.handle.net/11676/JoDR653JxQuqLvEwzqI2kdMw, Access Date: 22nd August, 2022.

Levin, I., Karstens, U., Hammer, S., DellaColetta, J., Maier, F., and Gachkivskyi, M. (2021): Limitations of the radon tracer method (RTM) to estimate regional greenhouse gas (GHG) emissions – a case study for methane in Heidelberg, Atmos. Chem. Phys., 21, 17907–17926, doi:10.5194/acp-21-17907-2021.

López-Coto, J., Mas, J. L., and Bolivar, J. P. (2013). A 40- year retrospective European radon flux inventory including climatological variability, Atmos. Environ., 73, 22–33, doi: 10.1016/j.atmosenv.2013.02.043.

López-Coto I., Mas J. L., Bolivar J. P., García-Tenorio A. (2009): A short-time method to measure the radon potential of porous materials. Applied Radiation and Isotopes 67, 133–138, doi: 10.1016/j.apradiso.2008.07.015.

Mclaughlin T. (2011): Technical Bases And Guidance For Radon Flux Monitoring At Uranium Mill Tailing Sites. DOE CONTRACT NO. DE-AC05-06OR23100, (RFTA 11-010) DCN 2042-TR-01-0

Millington, R. J. and Quirk, J. P. (1960). Transport in Porous media, Proceedings of the 7th International Congress of soil Science, Madison, Wisconsin, USA, 97–106.

Nazaroff, W. W. (1992). Radon transport from soil to air. Reviews of geophysics, 30(2), 137-160, doi: doi.org/10.1029/92RG00055.

Onishchenko, A., Zhukovsky, M., & Bastrikov, V. (2015). Calibration system for measuring the radon flux density. Radiation protection dosimetry, 164(4), 582-586, doi: 10.1093/rpd/ncv315.

Porstendörfer, J. (1994). Properties and behaviour of radon and thoron and their decay products in the air. Journal of Aerosol Science, 25(2), 219-263, doi: 10.1016/0021-8502(94)90077-9.

Prasad, G., Ishikawa, T., Hosoda, M., Sorimachi, A., Janik, M., Sahoo, S. K., ... & Uchida, S. (2012). Estimation of radon diffusion coefficients in soil using an updated experimental system. Review of Scientific Instruments, 83(9), 093503, doi: 10.1063/1.4752221.

Quindos, L. S., Fernandez, P. L., & Soto, J. (1994). A method for the measurement of the emanation factor for ^{222}Rn in small samples of porous materials. Radiation Protection Dosimetry, 56(1-4), 171-173, ISSN 0144-8420.

Rábago, D. Quindós, L. Vargas, Sainz, C. Radulescu, I. Ioan, I. Cardellini, F. Capogni, M. Celaya, S. Fuente, M. Grossi, C. (2022). Intercomparison of Radon Flux Monitors at Low and at High Radium Content Areas under Field Conditions. International Journal of Environmental Research and Public Health, 19(7), 4213. doi: 10.3390/ijerph19074213.

Rogers, V. C., & Nielson, K. K. (1991). Multiphase radon generation and transport in porous materials. Health Physics, 60(6), 807-815, doi: 10.1097/00004032-199106000-00006.

Röttger, S. Röttger, A. Grossi, C. Vargas, A. Karstens, U. Cinelli, G. Chung, E. Kikaj, D. Rennick, C. Mertes, F. Radulescu I. (2022): Radon metrology for use in climate change observation and radiation protection at the environmental level. Advances in Geosciences, 57, pp. 37–47, doi: 10.5194/adgeo-57-37-2022.

Röttger, A. Röttger, S. Grossi, S. Vargas A. et al. (2021): New metrology for radon at the environmental level, Measurement Science and Technology, 32(12), 124008, doi: 10.1088/1361-6501/ac298d.

Schery, S. D. and Wasiolek, M. A. (1998). Radon and Thoron in the Human Environment, chap. Modeling Radon Flux from the Earth's Surface, World Scientific Publishing, Singapore, 207–217.

Schüßler, W. (1996). Effektive Parameter zur Bestimmung des Gasaustauschs zwischen Boden und Atmosphäre, PhD thesis, Heidelberg University, Germany.

Stefani, N. Likos, W. J. Asce, M. Benson, C. (2016). Evaluation of Two Methods for Measuring Radon Flux from Earthen Radon Barriers. Geo-Chicago 2016 GSP 273, 145-155, WoS Id:000389439100016

Stieff, L., Kotrappa, P., & Bigu, J. (1996). Passive E-perm radon flux monitors for measuring undisturbed radon flux from the ground. In Proc. International Radon Symposium, American Assoc. of Radon Scientists and Technologists, Haines City, FL.

Stoulos, S., Manolopoulou, M., Papastefanou, C. (2004). Measurement of radon emanation factor from granular samples: effects of additives in cement. Applied Radiation and Isotopes, 60(1), 49-54, doi: 10.1016/j.apradiso.2003.10.004.

Szegvary, T., Conen, F., Ciais, P. (2009): European 222Rn inventory for applied atmospheric studies, Atmos. Environ., 43, 1536–1539, doi: 10.1016/j.atmosenv.2008.11.025.

Tan, Y., & Xiao, D. (2011). Revision for measuring the radon exhalation rate from the medium surface. IEEE Transactions on Nuclear Science, 58(1), 209-213, doi: 10.1109/TNS.2010.2090897.

Tan, Y., & Xiao, D. (2013). A novel method to measure the radon exhalation rate in only one measurement cycle. Analytical Methods, 5(3), 805-808, doi: 10.1039/C2AY26134K.

Tan, Y., Yuan, H., Xie, Y., Liu, C., Liu, X., Fan, Z., & Kearfott, K. (2020). No flow meter method for measuring radon exhalation from the medium surface with a ventilation chamber. Applied Radiation and Isotopes, 166, 109328, doi: 10.1016/j.apradiso.2020.109328.

UNSCEAR. United Nations Scientific Committee on the Effects of Atomic Radiation. (1988). *Sources, effects and risks of ionizing radiation*. New York. ISBN 92-1- 142143-8.

Yang J., Buchsteiner M., Salvamoser J., Irlinger J., Guo Q. And Tschiersch J. (2017) Radon Exhalation From Soil And Its Dependence From Environmental Parameters, Radiation Protection Dosimetry 177,1-2, 21–25, doi:10.1093/Rpd/Ncx165.

Zahorowski, W. and Whittlestone, S. (1996). A fast portable emanometer for field measurements of radon and thoron flux. Radiation Protection Dosimetry, 67, 2, 109-120, doi: 10.1093/oxfordjournals.rpd.a031802.

Zhang, B. Liu, H. Crawford, J.H. Chen ,G. Fairlie, T.D. Chambers, S.D. Kang, C.-H. Williams, A.G. Zhang, K. Considine, D.B. Sulprizio, M.P. Yantosca, R.M. (2021): Simulation of radon-222 with the GEOS-Chem global model: Emissions, seasonality, and convective transport, Atmospheric Chemistry and Physics 21, 1861-1887, doi:10.5194/acp-21-1861-2021.

Zhuo, W., Iida, T., and Furukawa, M. (2006): Modeling radon flux density from the Earth's surface, J. Nucl. Sci. Technol., ISSN 0022-3131, 43(4), 479-482.

Zhuo, W., Guo, O., Chen, B., and Cheng, G. (2008): Estimating the amount and distribution of radon flux density from the soil surface in China, J. Environ. Radioactiv., 99, 1143–1148, doi: 10.1016/j.jenvrad.2008.01.011.